Contrib. Astron. Obs. Skalnaté Pleso **56/2**, 7 – 35, (2026)
https://doi.org/10.31577/caosp.2026.56.2.7

Formation of Al II lines and photospheric aluminium abundances in B-type stars

Y. Takeda

11-2 Enomachi, Naka-ku, Hiroshima-shi, 730-0851, Japan (E-mail: ytakeda@js2.so-net.ne.jp)

Received: April 14, 2025; Accepted: May 7, 2025

Abstract. The aluminium abundances of early-to-late B-type main-sequence stars in the effective temperature range of $10000\,\mathrm{K} \lesssim T_{\rm eff} \lesssim 22000\,\mathrm{K}$ (comprising normal stars as well as chemically peculiar HgMn stars) were spectroscopically determined, with an aim of getting information about the galactic gas composition at the time of their formation from their photospheric abundances. For this purpose, two Al II lines at 6243 and 4663 Å were employed, for which the non-LTE effect was taken into account based on detailed statistical-equilibrium calculations. The non-LTE effect of these Al II lines generally acts in the direction of weakening (i.e., profile becomes shallower) caused by a decrease of line opacity (due to overionization) along with an enhanced line source function (overexcitation), and this effect tends to become progressively larger with an increase in $T_{\rm eff}$ as well as with a decrease in $\log g$ (surface gravity). Regarding the Al II 6243 line, while the non-LTE calculation qualitatively reproduces its overall behavior (e.g., transition from absorption to emission at early B-type), some $T_{\rm eff}$-dependent systematic trend remains unremoved in the non-LTE abundances of normal stars, which means that non-LTE corrections evaluated for this line are quantitatively insufficient. Meanwhile, for the case of the Al II 4663 line, which is more advantageous than the 6243 line in the sense that it is stronger without showing any emission, the resulting non-LTE abundances of ordinary B stars are almost constant at the solar abundance ($A \simeq 6.5$) over the wide $T_{\rm eff}$ range ($\sim$ 10000–20000 K), suggesting that the abundances derived from this line are successfully non-LTE-corrected and trustable. Therefore, according to the results from the Al II 4663 line, we may conclude that the Al abundance of the galactic gas in the recent past (several times $\sim 10^7$–10^8 yr ago) is almost consistent with the solar composition. As to the Al abundances of HgMn stars ($T_{\rm eff} \lesssim 15000\,\mathrm{K}$), our analysis confirmed that this element is conspicuously deficient (by $\sim$ 0.5–2 dex in comparison with the Sun) in the photosphere of these chemically peculiar stars, as already reported in previous studies.

Key words: line: formation – stars: abundances – stars: atmospheres – stars: chemically peculiar – stars: early-type

1. Introduction

Aluminium (Al; $Z = 13$) is one of the intermediate elements of astrophysical importance, which is considered to be synthesized mainly during the hydrostatic carbon and neon burning within massive stars and expelled outwards by type II supernovae explosion. While its chemical abundances have been rather well determined for a number of late-type (F–G–K) stars in a wide range of metallicity (e.g., Baumüller & Gehren (1997); Andrievsky et al. (2008); and the references therein), the situation is still insufficient in the field of early-type (A–B) stars. Unlike the case of cool solar-type stars where lines common to solar abundance determination may be used for deriving [Al/H] (differential abundance relative to the Sun), what matters more seriously in the case of hot stars is the reliability of absolute abundances which are not easy to establish precisely. Especially, since most of the previous studies have been done under the conventional assumption of LTE (Local Thermodynamic Equilibrium), an inadequacy of this presumption (neglect of the non-LTE effect) may be counted as a possible source of systematic error.

Given this situation, Takeda (2023) (hereinafter referred to as Paper I) tried to determine Al abundances of A-type stars ($7000\,\mathrm{K} \lesssim T_{\rm eff} \lesssim 10000\,\mathrm{K}$) based on the Al I 3944/3961 resonance lines by taking into account the non-LTE effect, because LTE abundances derived by past investigators were suspected to be considerably underestimated. It revealed in Paper I that this doublet suffers an appreciable non-LTE line-weakening and the serious zero-point discrepancy could be successfully removed ([Al/H] ~ 0 for [Fe/H] ~ 0 stars) by applying the significant (positive) non-LTE corrections amounting to up to $\lesssim 1$ dex.

As the follow-up of Paper I, the present study focuses on B-type stars ($10000\,\mathrm{K} \lesssim T_{\rm eff} \lesssim 22000\,\mathrm{K}$), but the intended scope is somewhat different. Most comparatively sharp-lined A-type stars (for which spectroscopic abundance determinations are feasible) more or less show some kind of chemical peculiarity (CP), and thus "normal" A stars are difficult to find in practice. In contrast, B-type main-sequence stars are divided rather clearly into non-CP (normal) stars and CP stars (mainly HgMn stars of late B-type), and we may expect the former "ordinary B stars" to retain the original gas at the time of star formation. Therefore, it may be possible to get the compositional information of the galactic gas in the recent past ($\sim 10^{7-8}$ yr ago when these B-type stars of ~ 3–$9\,M_\odot$ were formed) from the the photospheric abundances of normal B stars.

However, Al abundance determinations of B-type stars seem to have been more focused on chemically peculiar HgMn stars because of their anomalous aspects, for which considerable Al-deficiency has been almost established (see the compilation of Ghazaryan & Alecian (2016)). Meanwhile, our understanding on the abundances of this element for normal B stars in comparison with the Sun (are they consistent with the solar abundance?) is still unsatisfactory, because published results (all derived with the assumption of LTE) tend to be diversified

depending upon the adopted lines (UV or optical; Al I or Al II or Al III), as summarized below (though this literature survey may not be complete).

- Al abundance determinations for the well-studied benchmark sharp-lined star ι Her (B3 IV) have been reported by several authors, as compiled by Golriz & Landstreet (2017) (cf. Table 1 therein). While most of them are around A[1]$\sim$ 6.5 and consistent with the solar abundance ($A_\odot$ = 6.47),[2] Pintado & Adelman (1993) derived an appreciably discrepant result (A = 5.97) from the Al II 4663 line (though they obtained a near-solar averaged abundance of $\langle A \rangle \sim 6.5$ from four Al III lines).

- Pintado & Adelman (1993) also determined the Al abundance of γ Peg (B2 IV) and found that both Al II and Al III lines yielded a consistent abundance of $\langle A \rangle \sim 6.0$–6.1 (subsolar by several tenths dex).

- In Allen (1998)'s abundance studies on early A and late B stars, attempts of Al abundance determinations for normal late B-type stars (21 Peg, ζ Dra, 21 Aql, τ Her) based on Al I 3944/3961 and Al II 4663 lines yielded $A \sim 6.3$–6.4 (almost solar or slightly subsolar), while five HgMn stars were confirmed to be considerably Al-deficient (by $\sim$ 1 dex or even more).

- Fossati et al. (2009) determined Al abundances of two normal late B-type stars (21 Peg and π Cet) and obtained [Al/H][3] $\sim$ 0 dex (almost solar) for both, though the abundance from Al III lines (measured only for π Cet) turned out appreciably higher by $\sim$ 0.4 dex.

- Niemczura et al. (2009) conducted an extensive abundance study on a number of late B-type stars (including chemically peculiar stars). Although distinction of normal and peculiar stars is not clear in their sample and the adopted lines are not explicitly described, the Al abundances they obtained range widely from $A \sim 5.1$ to ~ 6.8.

- The Al abundances of the B-type supergiant β Ori (B8 Iae) derived by Przybilla et al. (2006) show an appreciable discrepancy between Al II (6.14$\pm$0.08) and Al III (7.00 $\pm$ 0.38) lines.

- Monier (2022) carried out an Al abundance analysis for HD 209459 (whether it is normal or peculiar is still controversial) based on the Al II 4663 line in the optical region and the Al III 1854/1862 resonance lines in the ultraviolet

[1] A is the logarithmic number abundance of the element relative to that of hydrogen (H) with the usual normalization of A(H) = 12.

[2] In this article, Anders & Grevesse (1989)'s solar photospheric Al abundance of $A_\odot = 6.47$ is adopted as the reference, in order to keep consistency with Kurucz (1993)'s ATLAS9/WIDTH9 program. This is fairly close to values given in Asplund et al. (2009)'s Table 1 (6.45 $\pm$ 0.03 for the solar photosphere, 6.43 $\pm$ 0.01 for the meteorites).

[3] As usual, [X/H] is the differential abundance of element X relative to the Sun; i.e., [X/H] $\equiv A_{\rm star}$(X) $- A_\odot$(X).

region. He found that, while the the strength of the former optical line is consistent with the solar Al abundance, a significantly reduced Al abundance ($\sim$30% of the solar composition) is needed to reproduce the strength of the latter UV lines.

Recently, Takeda (2024) (hereinafter referred to as Paper II) determined the phosphorus abundances of B-type stars by using the P II 6043 line while taking into account the non-LTE effect, and found that the non-LTE P abundances of superficially normal early-to-late B-type stars (formed several times $\sim 10^7$–10^8 yr ago) are systematically lower than the abundance of the Sun (its age is $\sim 4.6\times10^9$ yr) by $\sim$0.2–0.3 dex. This is a significant conclusion, because it means that the galactic gas composition of P has decreased with time, in contradiction to the general concept of chemical evolution.

It is, therefore, worthwhile to examine how the abundances of Al (intermediate element similar to P) in normal B-type stars are compared with that of the Sun (near-solar as usually expected? or subsolar like the case of P?), since published determinations are too insufficient to answer this question as mentioned above.

This situation motivated the author to contend with the task of Al abundance determinations for the same sample of B-type stars as investigated in Paper II. This is the purpose of the present study. Towards this aim, special attention is paid to the following points in context of the unsatisfactory results of past publications.

– One of the reasons for the confusingly diversified literature results may be the mixed use of various kinds of Al lines for abundance determination. In order to make things simple, we restrict ourselves in this investigation to two Al II lines in the optical region at 6243 and 4663 Å, both of which are observable from early- through late-B stars of wide $T_{\rm eff}$ range and of sufficiently high quality (e.g., neither too strong nor too weak, almost free from blending).

– The non-LTE effect is taken into account in deriving the abundances from these Al II lines. This may be significant, because previous Al abundance determinations for B stars mentioned above were done under the assumption of LTE. Of course, there is no guarantee that computed non-LTE corrections are reliable, since statistical-equilibrium calculations may often be imperfect due to uncertainties in the adopted atomic model. Yet, the validity of the non-LTE calculation can be checked by examining whether the resulting non-LTE Al abundances of normal B-type stars do not show any systematic dependence upon $T_{\rm eff}$ (most important parameter), which actually makes a useful touchstone.

Table 1. Atomic data of important lines.

Species	Mult. No.	Transition	λ (Å)	$\chi_{\rm low}$ (eV)	$\log gf$ (dex)	Gammar (dex)	Gammas (dex)	Gammaw (dex)
Ti II	34	$a^2G_{9/2}$–$z^2G^o_{9/2}$	3900.539	1.131	−0.290	8.31	−6.49	−7.82
Al II	1	$^1P^o_1$–$^1D_2$	3900.675	7.421	−2.26*	9.22	(−5.95)	(−7.77)
Al II	2	$^1D_2$–$^1P^o_1$	4663.046	10.598	−0.284	7.99	(−5.53)	(−7.64)
Si II	–	$^2F^o_{7/2}$–$^2G_{7/2}$	6239.614	12.840	−1.359	8.59	−3.54	−7.25
		$^2F^o_{7/2}$–$^2G_{9/2}$	6239.614		+0.185			
		$^2F^o_{5/2}$–$^2G_{7/2}$	6239.665		+0.072			
Al II	10	$^3P^o_2$–$^3D_1$	6243.073	13.077	−1.250	(7.76)	−4.76	(−7.50)
		$^3P^o_2$–$^3D_2$	6243.203		−0.080			
		$^3P^o_2$–$^3D_3$	6243.367		+0.670			

All these data are taken from the VALD database (Ryabchikova et al., 2015), except for the $\log gf$ value of the Al II 3900.675 line, for which the NIST data was adopted instead (because the VALD value is likely to be unreliable; cf. Sect. 5.2.3). Note that the Al II 6243 line comprises three components belonging to the same multiplet. The data of the Ti II 3900.539 line (contaminating Al II 3900) and the Si II 6239 line (high-excitation line similar to Al II 6243) are also shown. After the first six self-explanatory columns, damping parameters are given in the last three columns, where the parenthesized values are calculated by Kurucz (1993)'s WIDTH9 program (by following the default treatment) because the data are not given in VALD:
Gammar is the radiation damping width (s^{-1}), $\log \gamma_{\rm rad}$.
Gammas is the Stark damping width (s^{-1}) per electron density (cm^{-3}) at 10^4 K, $\log(\gamma_{\rm e}/N_{\rm e})$.
Gammaw is the van der Waals damping width (s^{-1}) per hydrogen density (cm^{-3}) at 10^4 K, $\log(\gamma_{\rm w}/N_{\rm H})$.
*Taken from the NIST database.

2. Line-formation of Al II lines

2.1. Non-LTE calculations

Statistical-equilibrium calculations for Al II were carried out by using the model atom of 68 terms (up to $10p\,^3P^o$ at 146602 cm^{-1}) with 601 radiative transitions (cf. Sect. 2.1 in Paper I for more details). While the contribution of Al I was neglected because it is negligible in the atmosphere of B-type stars, that of Al III (32 terms) and Al IV (only the ground term) was taken into account in the number conservation of total Al atoms. As done in Paper I, the data of photoionization cross sections were taken from TOPbase (Cunto & Mendoza, 1992) for the lowest 10 Al II terms (while the hydrogenic approximation was applied for the remaining terms), and the collisional rates were evaluated by following the recipe described in Sect. 3.1.3 of Takeda (1991).

The non-LTE departure coefficients were calculated on a grid of 56 ($= 14 \times 4$) solar-metallicity model atmospheres resulting from combinations of fourteen $T_{\rm eff}$ values (9000, 10000, 11000, 12000, 13000, 14000, 15000, 16000, 17000, 18000, 19000, 20000, 22000, and 24000 K) and four $\log g$ values (3.0, 3.5, 4.0, and 4.5), while assuming $v_{\rm t} = 2\,{\rm km\,s^{-1}}$ (microturbulence) and the solar abundance of $A({\rm Al}) = 6.47$ ([Al/H] = 0) as the input Al abundance.[4]

[4]The effect of assigned Al abundance on departure coefficients is discussed in Sect. 5.1.

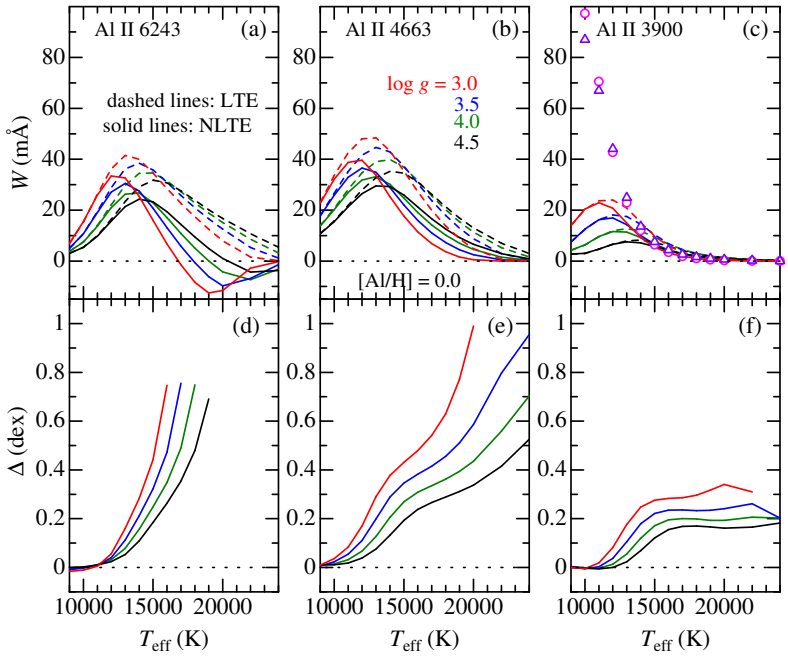

Figure 1. Non-LTE and LTE equivalent widths ($W^{\rm N}$ and $W^{\rm L}$ depicted in solid and dashed lines; upper panels (a)–(c)) and the corresponding non-LTE corrections (Δ; lower panels (d)–(f)), which were computed with the solar Al abundance on the non-LTE grid of models described in Sect 2.1, are plotted against $T_{\rm eff}$. Left ((a), (d)), center ((b), (e)), and right ((c), (f)) panels are for the Al II 6243, 4663, and 3900 lines, respectively. Results for different $\log g$ are distinguished by line colors (red, blue, green, black for 3.0, 3.5, 4.0, and 4.5). Note that Δ can not be calculated for the case of $W^{\rm N} \leq 0$ (because LTE abundance is unable to determine). In panel (c), the expected strengths of the Ti II 3900.539 line (contaminating the Al II 3900 line), which were calculated with the solar Ti abundance ($A_{\odot}$(Ti) = 4.99) for $\log g$ = 3.0 (pink open circles) and 4.0 (violet open triangles) models, are also plotted against $T_{\rm eff}$ for comparison.

2.2. Theoretical profiles and strengths of Al II lines

Now that the departure coefficients have been computed, the profile and strength of any line can be computed. Here, attention is paid to three representative Al II lines at 6243, 4663, and 3900 Å. The former two (6243 and 4663) are the lines used for abundance determination, while the latter 3900 line was originally considered as a candidate of abundance indicator but eventually abandoned (cf. Sect. 5.2.3). The atomic data of these lines are summarized in Table 1.

Fig. 1 illustrates how the theoretical equivalent widths of these lines calculated in LTE ($W^{\rm L}$; dashed line) as well as in non-LTE ($W^{\rm N}$; solid line) and

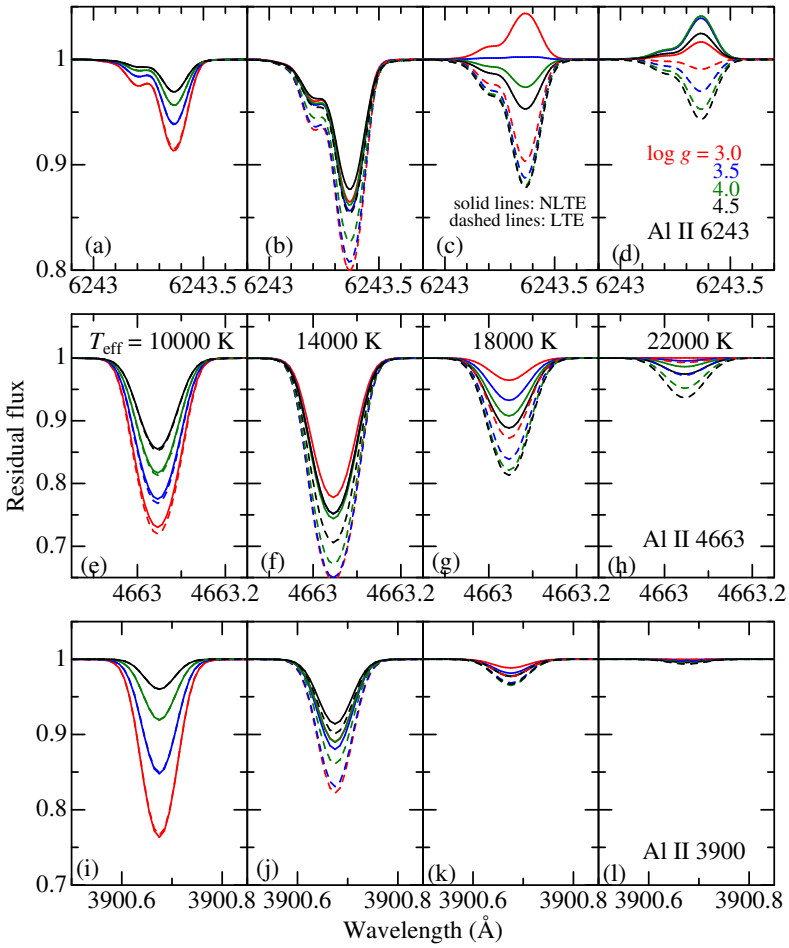

Figure 2. Theoretical line profiles computed for the Al II 6243 (top panels (a)–(d)), 4663 (middle panels (e)–(h)), and 3900 (bottom panels (i)–(l)) lines, each corresponding to $T_{\rm eff}$ = 10000 K, 14000 K, 18000 K, and 22000 K (from left to right). The same meanings of the line types and line colors as in Fig. 1.

the non-LTE corrections ($\Delta \equiv A^{\rm N} - A^{\rm L}$, where $A^{\rm L}$ and $A^{\rm N}$ are the abundances derived from $W^{\rm N}$ with LTE and non-LTE) depend upon $T_{\rm eff}$ and $\log g$. Likewise, the non-LTE and LTE profiles of these lines for the models of different $T_{\rm eff}$ values (10000, 14000, 18000, and 22000 K) are shown in Fig. 2.

The following characteristics are observed from these figures.

- The non-LTE effect acts as a line-weakening mechanism ($W^{\rm N} < W^{\rm L}$; Fig.1 and 2), which results in positive non-LTE corrections ($\Delta > 0$).

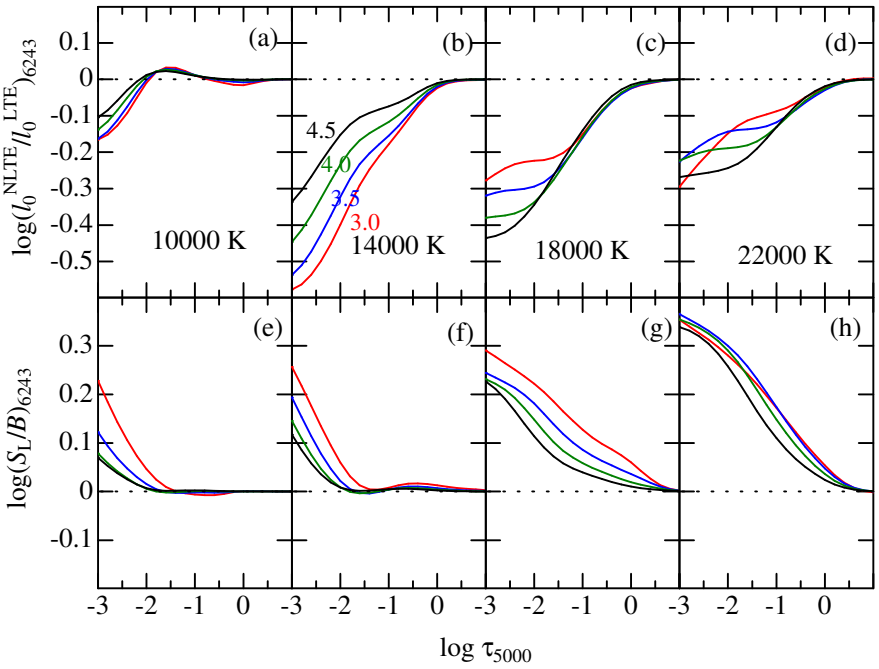

Figure 3. The non-LTE-to-LTE line-center opacity ratio (upper panels (a)–(d)) and the ratio of the line source function ($S_{\rm L}$) to the local Planck function (B) (lower panels (e)–(h)) for the Al II ^{3}P$^{\rm o}$–^{3}D transition (corresponding to Al II 6243) of multiplet 10, plotted against the continuum optical depth at 5000 Å. Shown here are the calculations done with $v_{\rm t} = 2\,{\rm km\,s^{-1}}$ and the solar Al abundance ([Al/H] = 0) for four representative $T_{\rm eff}$ values (from left to right): 10000 K (panels (a), (e)), 14000 K (panels (b), (f)), 18000 K (panels (c), (g)), and 22000 K (panels (d), (h)). The same meanings of the line colors as in Fig. 1.

- The non-LTE corrections (Δ) tend to increase towards higher $T_{\rm eff}$ and with a decrease in $\log g$ (Fig. 1).

- The overall behavior of W is qualitatively rather similar to each other with a peak around $T_{\rm eff} \sim 12000$–14000 K (though quantitatively $W_{3900} < W_{6243} < W_{4663}$).

- However, an emission feature emerges in the non-LTE profile of Al II 6243 line at $T_{\rm eff} \gtrsim 17000$ K (leading to $W^{\rm N}_{6243} < 0$), despite that the other two 4663 and 3900 lines retain ordinary absorption profiles.

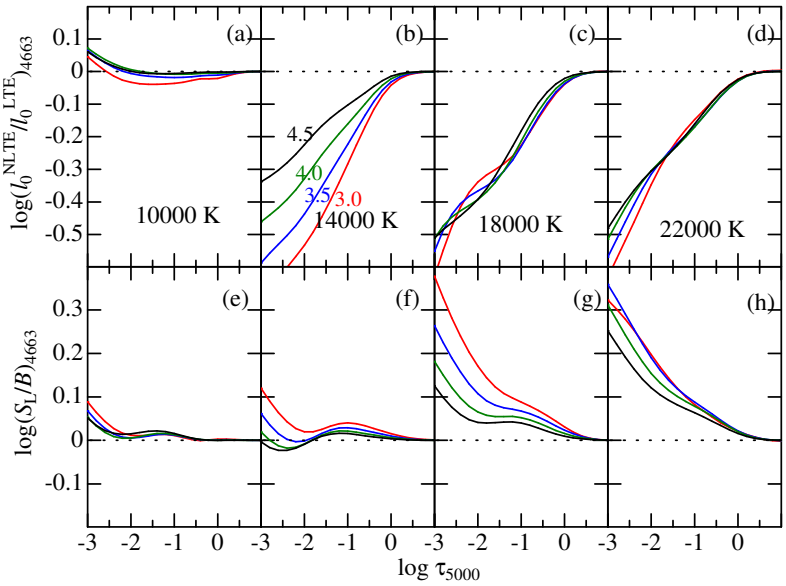

Figure 4. The non-LTE-to-LTE line-center opacity ratio and the ratio of the line source function (S_L) to the local Planck function (B) for the Al II ^{1}D–^{1}P$^\mathrm{o}$ transition (corresponding to Al II 4663) of multiplet 2, plotted against the continuum optical depth at 5000 Å. Otherwise, the same as in Fig. 3.

2.3. Physical mechanism of the non-LTE effect

In order to understand the behaviors of the non-LTE effect described in Sect. 2.2, the non-LTE-to-LTE line-center opacity ratio $l_0^\mathrm{NLTE}/l_0^\mathrm{LTE}$ ($\simeq b_\mathrm{l}$) and the ratio of the line source function to the Planck function S_L/B ($\simeq b_\mathrm{u}/b_\mathrm{l}$,[5] where b_l and b_u are the departure coefficients of lower and upper levels) for the transitions relevant to Al II 6243, 4663, and 3900 lines are plotted against the optical depth in Fig. 3, 4, and 5, respectively.

We can see from these figures that $l_0^\mathrm{NLTE}/l_0^\mathrm{LTE} < 1$ (overionization) and $S_\mathrm{L}/B > 1$ (overexcitation) in the line-forming region. This explains why the strengths of these lines are generally decreased by the non-LTE effect in B-type stars ($W^\mathrm{N} < W^\mathrm{L}$), because both conditions act in the direction of weakening the absorption profile.

Especially, the latter effect ($S_\mathrm{L}/B > 1$) plays a comparatively more significant role in this line weakening, which becomes more conspicuous with an increase in T_eff. Actually, the value of S_L/B in the line-forming region (e.g., at $\tau_{5000} \sim 0.1$) tends to be progressively larger towards higher T_eff (see pan-

[5]This relation holds under the condition that the photon energy $h\nu$ (h: Planck constant, ν: frequency) is not small in comparison with kT (k: Boltzmann constant). See also footnote 6.

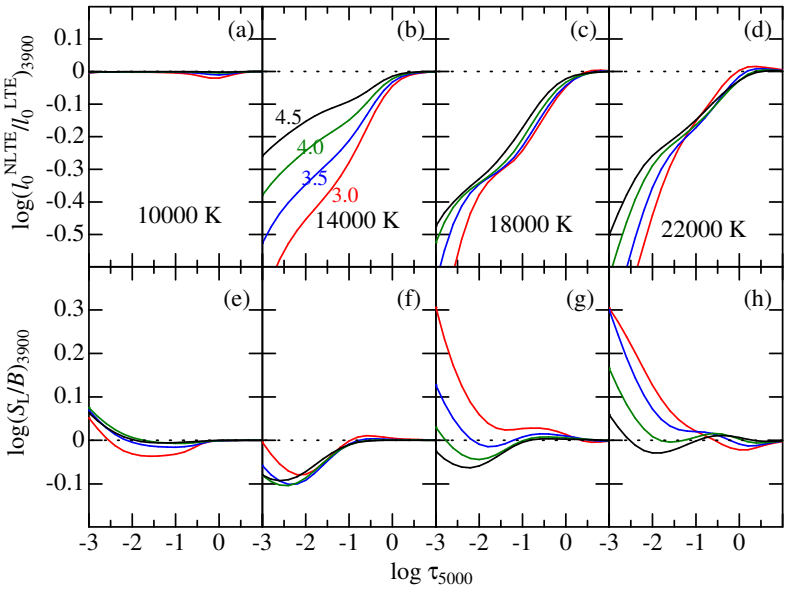

Figure 5. The non-LTE-to-LTE line-center opacity ratio and the ratio of the line source function ($S_{\rm L}$) to the local Planck function (B) for the Al II ^{1}P$^{\rm o}$–^{1}D transition (corresponding to Al II 3900) of multiplet 1, plotted against the continuum optical depth at 5000 Å. Otherwise, the same as in Fig. 3.

els (f)→(g)→(h) in Fig. 3 or Fig. 4), which eventually results in the trend of increasing Δ with $T_{\rm eff}$.

The cause of such an overexcitation ($S_{\rm L}/B > 1$) may be interpreted as that the lower level is more overionized than the upper level. Generally, overionization takes place when the photoionization rate ($\propto J_\lambda \sim W_{\rm D}B_\lambda(T_{\rm R})$) outweighs the recombination rate ($\propto B_\lambda(T_{\rm e})$) as $W_{\rm D}B_\lambda(T_{\rm R}) > B_\lambda(T_{\rm e})$, where $T_{\rm R}$ is the radiation temperature ($\simeq$ temperature of the continuum forming region), $W_{\rm D}$ is the dilution factor, and $T_{\rm e}$ is the electron temperature of the line-forming region. Since this inequality critically depends upon the T-sensitivity of B_λ, overionization is more enhanced at shorter wavelength regions (where B_λ is more sensitive to T). Accordingly, the fact that the wavelength of the photoionization edge for the lower level of a line is shorter than that for the upper level leads to $b_{\rm l} < b_{\rm u} (< 1)$; i.e., $S_{\rm L} > B$.

The appearance of an emission feature in the Al II 6243 line at the high $T_{\rm eff}$ range ($\gtrsim$ 17000 K) resulting from our non-LTE calculation (Fig. 2c and 2d) is also due to this effect of appreciably larger $S_{\rm L}$ over B, as recognized from Fig. 3g and 3h. The reason why this line shows an emission in the regime of early B-type may presumably be related to its longer wavelength than the other two, because the departure of $S_{\rm L}$ from B tends to be further enhanced in the Rayleigh–Jeans

region ($h\nu/kT < 1$).[6] It is worth noting that the Si II 6239.6 line (which is a similar high-excitation line with $\chi_{\rm low} \simeq 13\,{\rm eV}$ like Al II 6243; cf. Table 1) also shows an emission in early-to-mid B-type stars (see Sect. 4.3 and Fig. 6).

3. Observational data

3.1. Program stars

The target stars adopted in this investigation for Al abundance determinations are the same as in Paper II, which are 85 early-to-late B-type (near-)main-sequence stars (comprising normal as well as HgMn peculiar stars) in the solar neighborhood. They are comparatively sharp-lined ($v_{\rm e} \sin i \lesssim 60\,{\rm km\,s^{-1}}$) and have masses in the range of $2.5 M_\odot \lesssim M \lesssim 9 M_\odot$. The list of these 85 program stars is given in Table 2.

3.2. Adopted spectra

Since the sample stars in Paper II are targeted unchanged in this study, it is natural to use the same observational data (high-dispersion spectra obtained at Okayama Astrophysical Observatory) as adopted therein (see Sect. 2 in Paper II for the details). However, since the wavelength range covered by these spectra are limited to visible–red (or near-IR) region ($\lambda \gtrsim 5000$ Å), they can be employed only for the analysis of Al II 6243 line in the orange region.

Accordingly, blue-region spectra necessary for the analysis of Al II 4663 line (or Al II 3900 line) had to be obtained from the public-open data of stellar spectra. After searching the databases of ESO, CFHT, and ELODIE, spectra of 51 stars (out of 85 program stars) were found to be available and thus downloaded. The details of these data (file names, etc.) are summarized in Table 3.

Table 2. Program stars and the results of analysis.

No.	HD#	HR#	$T_{\rm eff}$	$\log g$	$v_{\rm e} \sin i$	W_{6243}	$A^{\rm N}_{6243}$	Δ_{6243}	W_{4663}	$A^{\rm N}_{4663}$	Δ_{4663}	Remark
(1)	(2)	(3)	(4)	(5)	(6)	(7)	(8)	(9)	(10)	(11)	(12)	(13)
1	029248	1463	22651	3.58	46	[0.0]	···	···	(no obs. data)			(ii)
2	000886	0039	21667	3.83	9	−7.0	···	···	3.9	6.92	0.58	(i)
3	035708	1810	21082	4.09	26	−13.2	···	···	5.6	6.77	0.47	(i)
4	035039	1765	20059	3.69	10	−8.7	···	···	(no obs. data)			(i)
5	042690	2205	19299	3.81	12	−8.3	···	···	6.0	6.53	0.45	(i)
6	032249	1617	18890	4.13	40	[0.0]	···	···	(no obs. data)			(ii)
7	034447	1731	18480	4.10	9	[0.0]	···	···	8.6	6.44	0.36	(ii)
8	196035	7862	17499	4.36	35	[0.0]	···	···	(no obs. data)			(ii)

[6] Let us define a parameter β ($\equiv 1 - b_{\rm l}/b_{\rm u}$) in order to indicate the degree of non-LTE overexcitation (i.e., difference between $b_{\rm l}$ and $b_{\rm u}$), by which $S_{\rm L}/B$ is expressed as $\simeq 1/(1-\beta)$ in the often encountered case of $h\nu/kT > 1$ (cf. footnote 5). However, in the high T and low ν case of $h\nu/kT < 1$, an alternative relation $S_{\rm L}/B \simeq 1/(1-\beta/\delta)$ holds, where $\delta \equiv h\nu/kT (< 1)$. That is, the extent of non-LTE departure (β) is further exaggerated by a factor of $1/\delta (> 1)$. See Sect. 12-4 in Mihalas (1978) for more details.

Table 2. (continued)

No.	HD#	HR#	$T_{\rm eff}$	$\log g$	$v_{\rm e}\sin i$	W_{6243}	$A^{\rm N}_{6243}$	Δ_{6243}	W_{4663}	$A^{\rm N}_{4663}$	Δ_{4663}	Remark
(1)	(2)	(3)	(4)	(5)	(6)	(7)	(8)	(9)	(10)	(11)	(12)	(13)
9	043157	2224	17486	4.12	37	1.6	5.64	0.49	14.7	6.55	0.34	
10	160762	6588	17440	3.91	7	1.1	5.57	0.58	12.9	6.52	0.36	
11	223229	9011	17327	4.20	31	[0.0]	···	···	(no obs. data)			(ii)
12	176502	7179	16821	3.89	8	7.2	6.25	0.48	(no obs. data)			
13	041753	2159	16761	3.90	28	[0.0]	···	···	(no obs. data)			(ii)
14	025558	1253	16707	4.29	41	3.4	5.74	0.33	16.6	6.45	0.28	
15	044700	2292	16551	4.21	5	5.3	5.94	0.34	15.6	6.41	0.29	
16	186660	7516	16494	3.57	9	4.3	6.05	0.53	(no obs. data)			
17	181858	7347	16384	4.19	17	7.0	6.05	0.33	15.8	6.40	0.29	
18	023793	1174	16264	4.15	46	6.8	6.02	0.32	(no obs. data)			
19	185330	7467	16167	3.77	4	[0.0]	···	···	1.3	5.23	0.31	(ii)
20	027396	1350	16028	3.91	15	7.3	6.05	0.34	(no obs. data)			
21	034798	1753	15943	4.27	37	8.8	6.07	0.27	20.6	6.49	0.27	
22	184171	7426	15858	3.54	27	4.6	5.89	0.40	(no obs. data)			
23	198820	7996	15852	3.86	32	9.7	6.18	0.34	22.6	6.60	0.34	
24	030122	1512	15765	3.72	15	[0.0]	···	···	(no obs. data)			(ii)
25	020756	1005	15705	4.43	18	7.7	5.96	0.23	(no obs. data)			
26	037971	1962	15532	3.63	9	2.5	5.51	0.33	11.6	6.18	0.33	
27	026739	1312	15490	3.92	31	10.8	6.15	0.29	22.3	6.51	0.31	
28	209008	8385	15353	3.50	20	7.0	5.98	0.34	20.5	6.51	0.37	
29	028375	1415	15278	4.30	19	14.7	6.25	0.22	24.0	6.49	0.24	
30	011415	0542	15174	3.54	42	10.9	6.16	0.32	22.0	6.52	0.35	
31	147394	6092	14898	4.01	30	13.0	6.15	0.22	(no obs. data)			
32	019268	0930	14866	4.24	17	12.8	6.13	0.19	(no obs. data)			
33	189944	7656	14793	4.01	35	14.8	6.21	0.22	27.0	6.53	0.27	
34	181558	7339	14721	4.15	14	13.6	6.15	0.19	22.7	6.38	0.22	
35	224990	9091	14569	3.99	35	5.0	5.64	0.19	14.4	6.09	0.22	
36	175156	7119	14561	2.79	12	8.9	6.10	0.38	26.7	6.76	0.49	
37	199578	8022	14480	4.02	27	16.2	6.23	0.19	(no obs. data)			
38	209419	8403	14404	3.82	16	16.0	6.21	0.21	(no obs. data)			
39	202753	8141	14318	3.84	40	9.6	5.93	0.19	21.7	6.32	0.24	
40	023300	1141	14207	3.84	19	16.3	6.20	0.19	(no obs. data)			
41	182255	7358	14190	4.29	28	12.4	6.08	0.13	28.1	6.48	0.18	
42	041692	2154	14157	3.19	28	16.1	6.22	0.26	27.5	6.55	0.37	
43	049606	2519	14121	3.82	19	(< 1.7)	(< 5.1)	0.16	0.7	4.62	0.20	(iii)
44	212986	8554	14121	4.27	20	13.9	6.14	0.13	(no obs. data)			
45	016219	0760	14113	4.06	23	17.1	6.23	0.15	(no obs. data)			
46	188892	7613	14008	3.38	30	13.7	6.09	0.22	(no obs. data)			
47	206540	8292	13981	4.01	13	15.7	6.18	0.15	27.3	6.43	0.21	
48	191243	7699	13923	2.50	28	[0.0]	···	···	(no obs. data)			(ii)
49	210424	8452	13740	3.99	12	14.1	6.11	0.13	28.3	6.44	0.19	
50	201888	8109	13689	4.01	5	15.6	6.16	0.12	(no obs. data)			
51	011857	0561	13600	3.88	20	17.3	6.21	0.13	(no obs. data)			
52	053244	2657	13467	3.42	36	(< 2.2)	(< 5.2)	0.15	2.4	5.09	0.21	(iii)
53	155763	6396	13397	4.24	41	21.8	6.40	0.09	34.3	6.59	0.14	
54	173117	7035	13267	3.63	22	12.7	6.00	0.12	23.3	6.24	0.19	
55	017081	0811	13063	3.72	20	19.6	6.26	0.10	33.8	6.52	0.18	
56	023408	1149	12917	3.36	30	(< 1.7)	(< 5.0)	0.11	5.5	5.41	0.18	(iii)
57	196426	7878	12899	3.89	6	13.8	6.10	0.08	30.3	6.43	0.14	
58	179761	7287	12895	3.46	16	17.8	6.16	0.11	30.4	6.40	0.19	
59	011529	0548	12858	3.43	30	20.2	6.23	0.10	(no obs. data)			

Table 2. (continued)

No.	HD#	HR#	$T_{\rm eff}$	$\log g$	$v_{\rm e}\sin i$	W_{6243}	$A^{\rm N}_{6243}$	Δ_{6243}	W_{4663}	$A^{\rm N}_{4663}$	Δ_{4663}	Remark
(1)	(2)	(3)	(4)	(5)	(6)	(7)	(8)	(9)	(10)	(11)	(12)	(13)
60	178065	7245	12243	3.49	4	(<0.6)	(<4.6)	0.06	0.8	4.49	0.10	(iii)
61	038899	2010	10774	4.02	26	10.7	6.43	0.01	24.3	6.49	0.03	
62	043247	2229	10301	2.39	33	4.3	5.45	0.00	15.2	5.75	0.06	
63	209459	8404	10204	3.53	3	7.7	6.25	0.00	23.4	6.41	0.03	
64	181470	7338	10085	3.92	2	6.3	6.34	0.00	(no obs. data)			
65	098664	4386	10194	3.75	62	(<5.0)	(<6.1)	0.00	24.5	6.53	0.03	(iii)
66	130557	5522	10142	3.85	55	(<6.2)	(<6.3)	0.00	16.6	6.29	0.02	(iii)
67	079158	3652	13535	3.72	46	8.1	5.79	0.13	(no obs. data)			
68	106625	4662	11902	3.36	37	(<1.3)	(<4.9)	0.05	(no obs. data)			(iii)
69	150100	6184	10542	3.84	36	(<3.1)	(<5.8)	0.01	8.9	5.82	0.02	(iii)
70	197392	7926	13166	3.46	30	19.0	6.20	0.13	(no obs. data)			
71	198667	7985	11125	3.42	26	14.2	6.25	0.01	(no obs. data)			
72	202671	8137	13566	3.36	25	(<3.5)	(<5.4)	0.17	3.8	5.32	0.23	(iii)
73	193432	7773	10180	3.91	24	5.9	6.27	0.00	22.7	6.53	0.02	
74	161701	6620	12692	4.04	20	13.6	6.15	0.06	(no obs. data)			
75	077350	3595	10141	3.68	20	4.9	6.10	0.00	18.7	6.31	0.02	
76	129174	5475	12929	4.02	16	(<1.5)	(<5.1)	0.07	(no obs. data)			(iii)
77	201433	8094	12193	4.24	15	17.9	6.44	0.04	(no obs. data)			
78	144206	5982	11925	3.79	12	(<0.8)	(<4.8)	0.04	3.2	5.16	0.06	(iii)
79	145389	6023	11714	4.02	11	(<0.9)	(<5.0)	0.03	7.9	5.66	0.05	(iii)
80	190229	7664	13102	3.46	10	(<1.1)	(<4.8)	0.12	1.5	4.84	0.17	(iii)
81	149121	6158	10748	3.89	10	(<1.0)	(<5.2)	0.01	0.7	4.60	0.02	(iii)
82	078316	3623	13513	3.85	8	(<0.9)	(<4.8)	0.11	0.5	4.40	0.15	(iii)
83	089822	4072	10307	3.89	5	(<0.4)	(<5.0)	0.00	1.7	5.07	0.02	(iii)
84	143807	5971	10828	4.06	4	3.3	5.82	0.01	9.0	5.85	0.02	
85	193452	7775	10543	4.15	3	2.9	5.89	0.01	(no obs. data)			

(1) Star number (tentatively assigned). (2) Henry Draper Catalogue number. (3) Bright Star Catalogue number. (4) Effective temperature (in K). (5) Logarithmic surface gravity (in $\mathrm{cm\,s^{-2}}$/dex). (6) Projected rotational velocity (in $\mathrm{km\,s^{-1}}$). (7) Equivalent width of Al II 6243 line (in mÅ). (8) Non-LTE Al abundance derived from Al II 6243 (in dex). (9) Non-LTE correction for Al II 6243 (in dex). (10) Equivalent width of Al II 4663 line (in mÅ). (11) Non-LTE Al abundance derived from Al II 4663 (in dex). (12) Non-LTE correction for Al II 4663 (in dex). (13) Remarks for the unmeasurable cases of Al II 6243.
Since this table is so arranged as to be consistent with Table 1 of Paper II (which should be consulted for more details of the program stars), the first part (#1–#64) present the data of 64 early-to-late B stars (in the descending order of $T_{\rm eff}$) followed by the second part (#65–#85) for 21 late B-type stars (in the descending order of $v_{\rm e}\sin i$). Column (13) indicates the cases where Al abundances could not be established from the Al II 6243 line, which are divided into three types (cf. Sect. 4.3 and 4.4): (i) Line profiles show an appreciable emission feature (early-to-mid B-type stars). (ii) Lines are too weak because of filled-in emissions (early-to-mid B-type stars). (iii) Lines are too weak but considered to be due to very low Al abundance (late B-type HgMn stars).

Table 3. Public-open data additionally employed in this study.

Star No.	HD#	*Data/Instrument	File name	Remark
2	000886	ELODIE	elodie_19981123_0019.fits	
3	035708	CFHT/ESPaDOnS	1288837i.fits-1288844i.fits	8 files co-added
5	042690	ESO/FERROS	ADP.2016-09-27T09_50_43.972.fits	
7	034447	ESO/XSHOOTER	ADP.2017-08-11T08_26_08.731.fits	
9	043157	ESO/XSHOOTER	ADP.2017-08-10T15_20_15.958.fits	$R = 3250$
10	160762	CFHT/ESPaDOnS	1216549i.fits-1216568i.fits	20 files co-added
14	025558	CFHT/ESPaDOnS	1977059i.fits-1977070i.fits	12 files co-added
15	044700	ESO/XSHOOTER	ADP.2017-08-11T21_07_09.955.fits	
17	181858	ESO/XSHOOTER	ADP.2017-08-18T07_38_30.899.fits	$R = 5400$
19	185330	CFHT/ESPaDOnS	1266787i.fits-1266790i.fits	4 files co-added
21	034798	ESO/FERROS	ADP.2016-09-27T09_50_43.812.fits	
23	198820	ELODIE	elodie_20041110_0019.fits	
26	037971	ELODIE	elodie_20030113_0020.fits	
27	026739	ESO/FERROS	ADP.2016-09-23T06_51_12.898.fits	
28	209008	ESO/UVES	ADP.2020-07-20T14_03_10.973.fits	
29	028375	ESO/XSHOOTER	ADP.2017-08-11T22_53_23.592.fits	$R = 5400$
30	011415	CFHT/ESPaDOnS	1168487i.fits-1168490i.fits	4 files co-added
33	189944	ESO/XSHOOTER	ADP.2017-08-11T18_51_15.004.fits	
34	181558	ESO/HARPS	ADP.2014-09-17T11_21_34.070.fits	
35	224990	ESO/FERROS	ADP.2016-09-27T09_50_42.585.fits	
36	175156	ESO/UVES	ADP.2020-06-30T13_28_27.894.fits	
39	202753	ESO/HARPS	ADP.2014-09-23T11_05_18.230.fits	
41	182255	ELODIE	elodie_20031106_0018.fits	
42	041692	ESO/HARPS	ADP.2016-09-05T01_02_13.863.fits	
43	049606	CFHT/ESPaDOnS	2787264i.fits-2787267i.fits	4 files co-added
47	206540	ESO/XSHOOTER	ADP.2017-08-11T04_40_12.486.fits	
49	210424	ESO/UVES	ADP.2021-09-01T05_49_03.769.fits	
52	053244	ESO/FERROS	ADP.2016-09-21T07_46_52.316.fits	
53	155763	ELODIE	elodie_20010809_0017.fits	
54	173117	ESO/XSHOOTER	ADP.2018-09-13T17_16_55.500.fits	$R = 5400$
55	017081	ESO/UVES	ADP.2020-07-10T21_52_27.364.fits	
56	023408	ESO/FERROS	ADP.2016-09-27T09_50_43.630.fits	
57	196426	ESO/UVES	ADP.2020-08-04T20_45_41.082.fits	
58	179761	ESO/UVES	ADP.2020-08-04T15_46_04.184.fits	
60	178065	ESO/UVES	ADP.2020-08-14T10_13_40.490.fits	
61	038899	ESO/HARPS	ADP.2016-09-04T01_02_02.711.fits	
62	043247	ESO/FERROS	ADP.2016-09-27T09_50_43.636.fits	
63	209459	CFHT/ESPaDOnS	1649409i.fits-1649412i.fits	4 files co-added
65	098664	ESO/FERROS	ADP.2016-09-27T09_50_43.696.fits	
66	130557	ESO/UVES	ADP.2020-06-09T07_11_28.785.fits	
69	150100	ELODIE	elodie_19980704_0017.fits	
72	202671	ESO/FERROS	ADP.2016-09-27T09_50_43.826.fits	
73	193432	ESO/UVES	ADP.2020-08-14T10_35_52.467.fits	
75	077350	ELODIE	elodie_20050203_0013.fits	
78	144206	ELODIE	elodie_20000818_0006.fits	
79	145389	ELODIE	elodie_20040512_0019.fits	
80	190229	CFHT/ESPaDOnS	2770404i.fits-2770407i.fits	4 files co-added
81	149121	ESO/UVES	ADP.2020-06-12T15_23_23.451.fits	
82	078316	ESO/FERROS	ADP.2016-09-27T07_02_43.215.fits	
83	089822	CFHT/ESPaDOnS	2948464i.fits-2948467i.fits	4 files co-added
84	143807	ELODIE	elodie_20040510_0015.fits	

These are the data adopted for the analysis of the Al II 4663 line (also for checking the Al II 3900 line in HD 160762, HD 209008, and HD 209459; cf. Sect. 5.2.3). Although most of these spectra are of sufficiently high resolving power ($R \gtrsim 10000$), some are of medium spectral resolution (R is only several thousands) as remarked in the last column.
ESO $\cdots$ ESO Science Archive Facility (`https://archive.eso.org/cms.html`).
CFHT $\cdots$ Canada-France-Hawaii Telescope; data available from the Canadian Astronomy Data Centre (`https://www.cadc.hia.nrc.gc.ca/`).
ELODIE $\cdots$ The ELODIE Archive (`https://atlas.obs-hp.fr/elodie/`).

4. Abundance determination

4.1. Procedures

The abundances of Al for the program stars are determined by almost the same procedures as adopted in Paper I or Paper II, which consist of four steps. (1) First, the spectrum-fitting analysis is applied to two spectral regions comprising Al II 6243 and Al II 4663 lines, and the best fit parameter solutions are determined. (2) Based on such established abundance solutions, the equivalent widths of these two Al lines (W) are inversely calculated. (3) Then the non-LTE abundance ($A^{\rm N}$) is derived from W by taking into account the non-LTE effect. (4) Finally, uncertainties in the abundance results are estimated, while considering the errors in W along with the sensitivities to parameter changes.

4.2. Atmospheric parameters

Regarding the atmospheric parameters assigned to each star, the same values as used in Paper II (see Sect. 3 therein for the details) are adopted in this study. In Table 1 are shown the values of $T_{\rm eff}$ and $\log g$, which were originally determined from colors of the Strömgren system. As to the microturbulence, $v_{\rm t} = 1\,{\rm km\,s^{-1}}$ ($T_{\rm eff} < 16500\,{\rm K}$) and $2\,{\rm km\,s^{-1}}$ ($T_{\rm eff} > 16500\,{\rm K}$) are tentatively assumed as done in Paper II, which is sufficient because this parameter is practically insignificant in the present case (cf. Sect. 4.5). Likewise, the model atmospheres for each of the targets are the solar-metallicity models generated by interpolating Kurucz (1993)'s ATLAS9 model grid in terms of $T_{\rm eff}$ and $\log g$.

4.3. Synthetic spectrum fitting

The spectrum-fitting analysis (Takeda, 1995) by assuming LTE was applied to two wavelength regions (6230–6250 Å and 4656–4668 Å, each comprising Al II 6243 and 4663, respectively), in order to accomplish the best fit between theoretical and observed spectra. Here, the parameters varied are the chemical abundances (of Al and other elements showing appreciable lines), rotational broadening velocity ($v_{\rm e} \sin i$), and radial velocity ($V_{\rm rad}$). The data of all atomic lines (including those of Al lines given in Table 1) in each region were taken from the VALD database (Ryabchikova et al., 2015).

It then revealed that, while Al abundances could be successfully established for all 51 stars in the fitting analysis of the 4656–4668 Å region, its determination had to be abandoned for 29 stars (out of 85 stars) in the 6230–6250 Å region analysis since the Al II 6243 line did not exhibit any detectable absorption profile. This is due to the fact that this line begins to show an emission feature in the high $T_{\rm eff}$ regime of early-to-mid B-type stars, which is actually predicted in the non-LTE calculations (cf. Fig. 2c and 2d). In order to illustrate this situation, the spectral portions in the neighborhood of the Al II 6243 and 4663 lines for stars with $T_{\rm eff} \gtrsim 16000\,{\rm K}$ are displayed in Fig. 6, where we can see that the Al II

6243 line is not usable for a large fraction of stars at $T_{\rm eff} \gtrsim 17000$ K (because of being emission or very weak due to filled-in emission). Meanwhile, this 6243 line is too weak to be measurable in chemically peculiar HgMn stars (mostly late B-type) because Al is considerably deficient in their atmospheres.

Accordingly, those 29 stars for which Al abundance could not be derived from the 6243 line are divided into three categories: (i) emission line (early- or mid-B stars), (ii) very weak line due to the effect of filled-in emission (mid-B stars), and (iii) very weak line due to considerable Al-deficiency (late-B HgMn stars), as indicated in column 13 of Table 2. In such cases, the fitting was tentatively done either by masking the 6243 line region or by fixing the Al abundance at an arbitrary value. The cases (ii) and (iii) can be clearly distinguished from each other by checking the neighboring Si II 6239.6 line, because this Si II line also shows an emission (or filled-in emission) in the former case (ii), while not in the latter case (iii).

The comparison of theoretical spectrum (for the solutions with converged parameters) with the observed spectrum (for the selected wavelength region in the neighborhood of the relevant Al lines) is shown in Fig. 7 (6243 line region) and Fig. 8 (4663 line region) for each star.

4.4. Evaluation of equivalent widths

Next, the equivalent widths (W_{6243} and W_{4663}) of the Al II 6243 and 4663 lines were inversely evaluated from the Al abundance solution derived from the spectrum-fitting analysis (cf. Sect. 4.3) with the same model and atmospheric parameters, where Kurucz (1993)'s WIDTH9 program[7] was employed for this purpose. The errors involved in such obtained W values (δW) were further estimated from the line-center depth and the S/N ratio by applying Eq. (1) in Paper II, which are typically on the order of $\lesssim$1–2 mÅ in most cases (though up to several mÅ or more in exceptionally shallow/broad-line cases)

The resulting W_{6243} and W_{4663} for each star are presented in Table 2. Regarding 29 stars for which abundances could not be determined from the 6243 line (cf. Sect. 4.3), following values are assigned to W_{6243} in this table for each of the three cases (i, ii, iii). (i) W_{6243} (negative) was directly measured from the emission-line profile by the Gaussian fitting. (ii) Zero value (0) is tentatively given. (iii) An upper-limit value ($W^{\rm ul}_{6243}$) is presented, which was estimated from the line width and the S/N ratio by using Eq. (1) of Takeda (2025).

4.5. Non-LTE abundances and their uncertainties

Then, the non-LTE abundances ($A^{\rm N}_{6243}$ and $A^{\rm N}_{4663}$) were determined from W_{6243} and W_{4663} for each star by taking into account the departure from LTE, where

[7]The original WIDTH9 program was considerably modified by the author in various respects; for example, enabling the treatment of multi-component lines (such as the Al II 6243 line), inclusion of the non-LTE effect, etc.

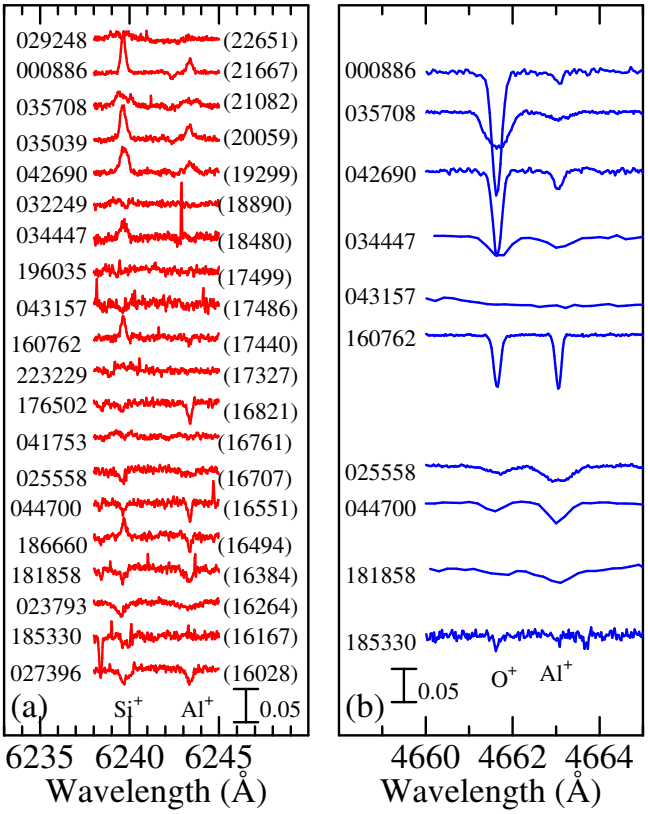

Figure 6. Observed spectra of the early-to-mid B-type stars with $T_{\rm eff} \gtrsim 16000\,{\rm K}$ in the neighborhood of (a) Al II 6243 line and (b) Al II 4663 line, which are designated by the HD number on the left and arranged in the descending order of $T_{\rm eff}$ (indicated by parenthesized values). Note that the Al II 6243 line (along with the neighboring Si II 6239 line) shows an emission or a very weak strength due to filled-in emission at $T_{\rm eff} \gtrsim 17000\,{\rm K}$, whereas the Al II 4663 line ever keeps an absorption profile.

the departure coefficients calculated on the grid of 56 models (cf. Sect. 2.1) were interpolated in terms of $T_{\rm eff}$ and $\log g$, from which the non-LTE corrections (Δ; difference of $A^{\rm N}$ from the LTE abundance $A^{\rm L}$) were also obtained. The resulting values of W, $A^{\rm N}$, and Δ for each line are given in Table 2. Likewise, W, $A^{\rm L}$, Δ and $A^{\rm N}$ are plotted against $T_{\rm eff}$ in panels ((a)–(d)) of Fig. 9 (6243) and Fig. 10 (4663), where the error bars attached in W (panel (a)) are $\pm\delta W$ (Sect. 4.4)

The abundance sensitivities to typical ambiguities in atmospheric parameters [$\delta_{T\pm}$ (abundance changes for $T_{\rm eff}$ perturbations by $\pm 3\%$), $\delta_{g\pm}$ (abundance changes for $\log g$ perturbations by $\pm 0.2\,{\rm dex}$), and $\delta_{v\pm}$ (abundance changes for $v_{\rm t}$

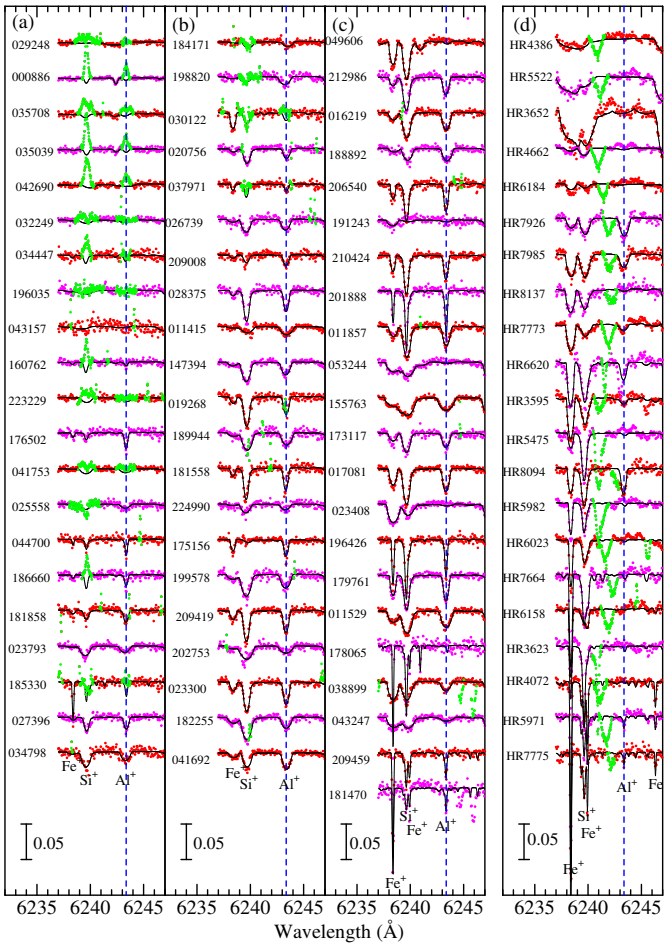

Figure 7. Synthetic spectrum-fitting in the neighborhood of the Al II 6243 line done for each of the 85 program stars. Shown here is the selected wavelength region of 6237–6247 Å. The best-fit theoretical spectra are depicted by black solid lines, while the observed data are plotted by colored dots (outlier data points rejected in calculating χ^2 are highlighted in light green). The spectra are arranged in the same manner as Fig. 3 of Paper II to keep consistency with that paper: Panels (a), (b), and (c) are for the 64 early-to-late B stars (indicated by the HD number) in the descending order of $T_{\rm eff}$ (from top to bottom; from left to right). while the rightmost panel (d) is for 21 late-B stars (indicated by the HR number) in the descending order of $v_{\rm e} \sin i$. An offset of 0.05 (in unit of the continuum) is applied to each spectrum relative to the adjacent one. The position of 6243.367 Å (wavelength of the strongest component of Al II 6243 triplet) is shown by the vertical dashed line. The wavelength scale is in the laboratory frame after correcting the radial velocity shift.

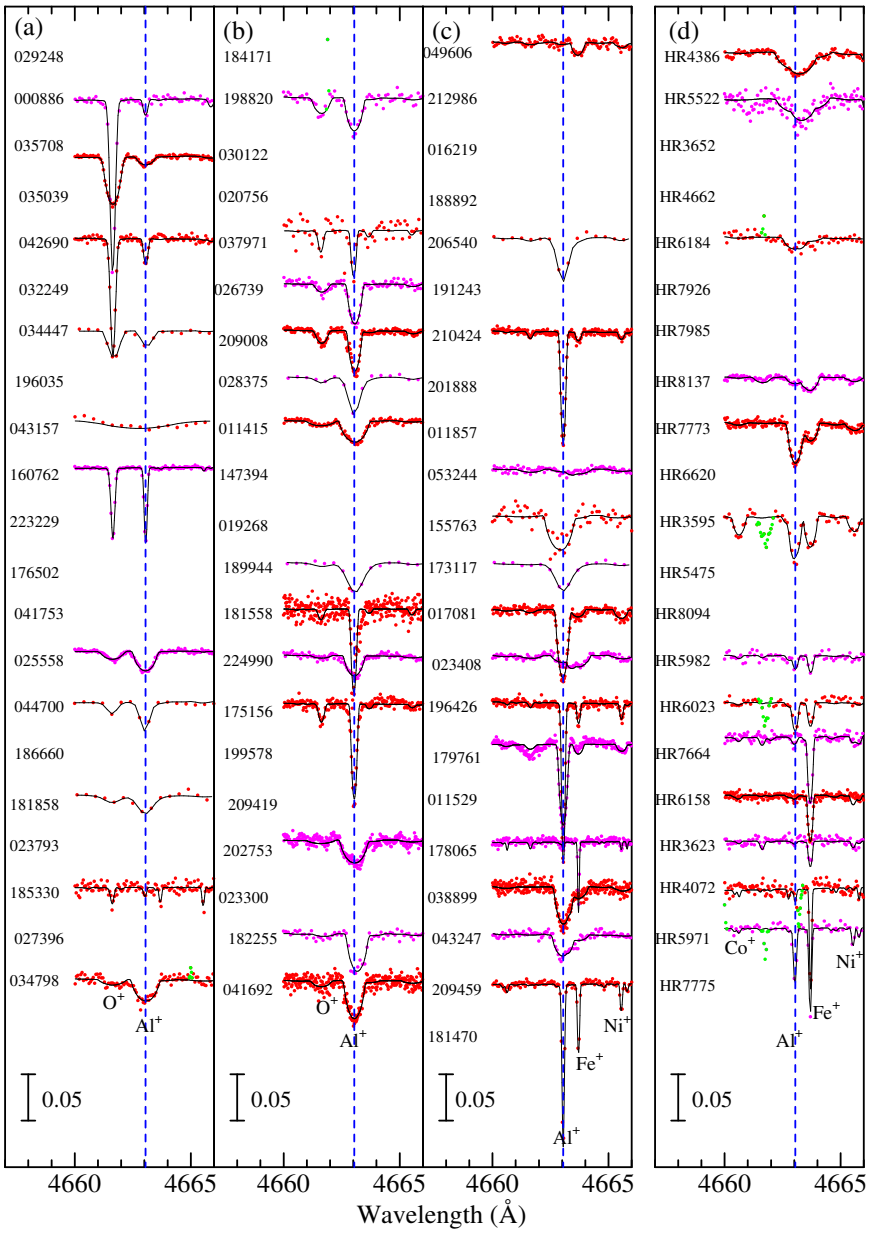

Figure 8. Synthetic spectrum-fitting in the neighborhood of the Al II 4663 line done for 51 stars, for which public-open data are available (cf. Table 3). Shown here is the selected wavelength region of 4660–4666 Å. The position of 4663.046 Å (wavelength of the Al II 4663 line) is shown by the vertical dashed line. Otherwise, the same as in Fig. 7.

perturbations by $\pm 1\,\mathrm{km\,s^{-1}}$)] are plotted against $T_{\rm eff}$ in panels (e)–(g) of Fig. 9 and Fig. 10. We can see from these figures that combined impacts of parameter uncertainties upon the abundances (due mainly to $T_{\rm eff}$ and partly to $\log g$, while the response to $v_{\rm t}$ change is negligibly small) are $\pm \lesssim 0.1$–0.2 dex at most. The error bars attached in $A^{\rm N}$ (panel (d)) are the root-sum-square of δA (abundance error due to W perturbation of $\pm\delta W$), δ_T, δ_g, and δ_v.

5. Discussion

5.1. Impact of assigned abundance in non-LTE calculations

Before discussing the results obtained in Sect. 4, some comments may be in order regarding the Al abundance adopted in non-LTE calculations (Sect. 2.1), which we assumed the solar abundance ([Al/H] = 0). Since the departure coefficients resulting from statistical-equilibrium calculations more or less depend upon the input abundance, its validity in an application to actual stars needs to be checked.

Originally, it was intended to derive several non-LTE abundances for a star corresponding to different sets of departure coefficients calculated with various [Al/H] values, and obtain the consistent abundance solution by interpolation as done in Paper II (cf. Sect. 6.2 therein). Unfortunately, this approach did not work well in the present case, because $A^{\rm N}_{6243}$ determination (for a given W_{6243}) was found to be not always successful if [Al/H] is changed.

This situation is illustrated in Fig. 11, where the non-LTE corrections (Δ_0, $\Delta_{-0.5}$, Δ_{-1}) for each star derived by applying three sets of departure coefficients (corresponding to [Al/H] = 0.0, −0.5, and −1.0) are plotted against $T_{\rm eff}$. An inspection of this figure reveals that, while Δ_{4663} is insensitive to a change in [Al/H] (Fig. 11b), Δ_{6243} is appreciably [Al/H]-dependent (i.e., increasing with a decrease in [Al/H]; cf. Fig. 11a). More seriously, Δ_{6243} tends to be indeterminable as [Al/H] is decreased, especially at higher $T_{\rm eff}$ (note that the number of Δ_{6243} plotted in Fig. 11a becomes progressively fewer with a decrease in [Al/H]). This stems from the fact that the non-LTE line-weakening effect (due to the growth of filled-in emission caused by an increase of $S_{\rm L}$) becomes more important with a decrease in [Al/H], particularly in the higher $T_{\rm eff}$ regime. In such cases, non-LTE $W^{\rm N}_{6243}$ may not necessarily be a monotonically increasing function of A any more, since even an increase of the abundance can "weaken" the line strength by the effect of filled-in emission as the line-forming region shifts towards higher. Therefore, the solution of $A^{\rm N}_{6243}$ corresponding to a given W_{6243} tends to be undetermined at higher $T_{\rm eff}$ if departure coefficients for lower [Al/H] are used.

However, our choice of applying the non-LTE departure coefficients calculated with [Al/H] = 0 to all stars is reasonably sufficient from a practical point of view for the following reasons.

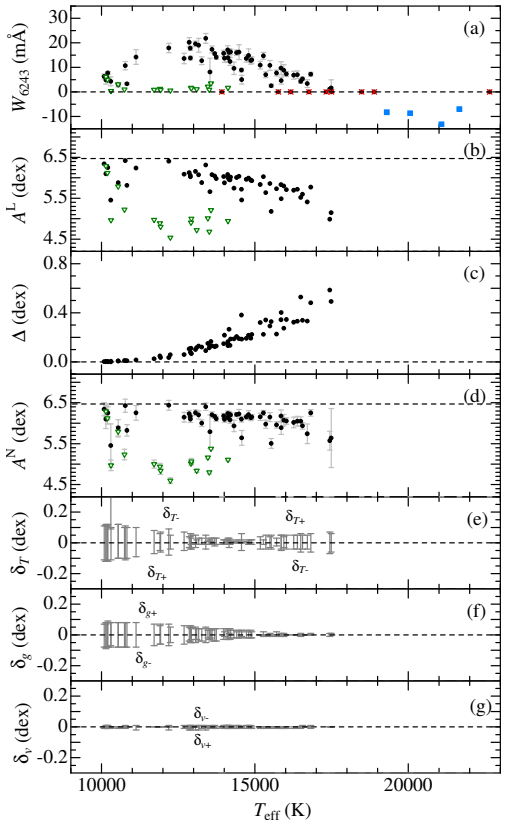

Figure 9. Abundance-related quantities for the Al II 6243 line are plotted against $T_{\rm eff}$. (a) W_{6243} (equivalent width), where the indicated error bars ($\pm\delta W$) are their uncertainties (see Sect. 4.4). (b) $A^{\rm L}$ (LTE aluminium abundance). (c) Δ ($\equiv A^{\rm N} - A^{\rm L}$; non-LTE correction). (d) $A^{\rm N}$ (non-LTE aluminium abundance). Here, the attached error bars are the root-sum-squares of δ_W (abundance ambiguities corresponding to δW), δ_T, δ_g, and δ_v. (e) δ_{T+} and δ_{T-} (abundance variations in response to $T_{\rm eff}$ changes of +3% and −3%). (f) δ_{g+} and δ_{g-} (abundance variations in response to $\log g$ changes of +0.2 dex and −0.2 dex). (g) δ_{v+} and δ_{v-} (abundance variations in response to perturbing the standard $v_{\rm t}$ value by $\pm 1\,{\rm km\,s^{-1}}$). Note that the signs of δ_T and δ_g are reversed on both sides of $T_{\rm eff}$ around ~ 15000 K. In panels (a), (b), and (d), the three cases where W or A values could not orderly be established (cf. Sect. 4.3 and 4.4) are distinguished by differently colored symbols: blue squares ⋯ (negative) W values directly measured by Gaussian fitting (appreciable emission-line case (i)); overplotted red crosses ⋯ tentatively assigned zero values (too weak line case (ii) due to filled-in emission in mid- to early-B stars); green open downward triangle ⋯ upper limit values (too weak line case (iii) due to Al deficiency in late B-type HgMn stars).

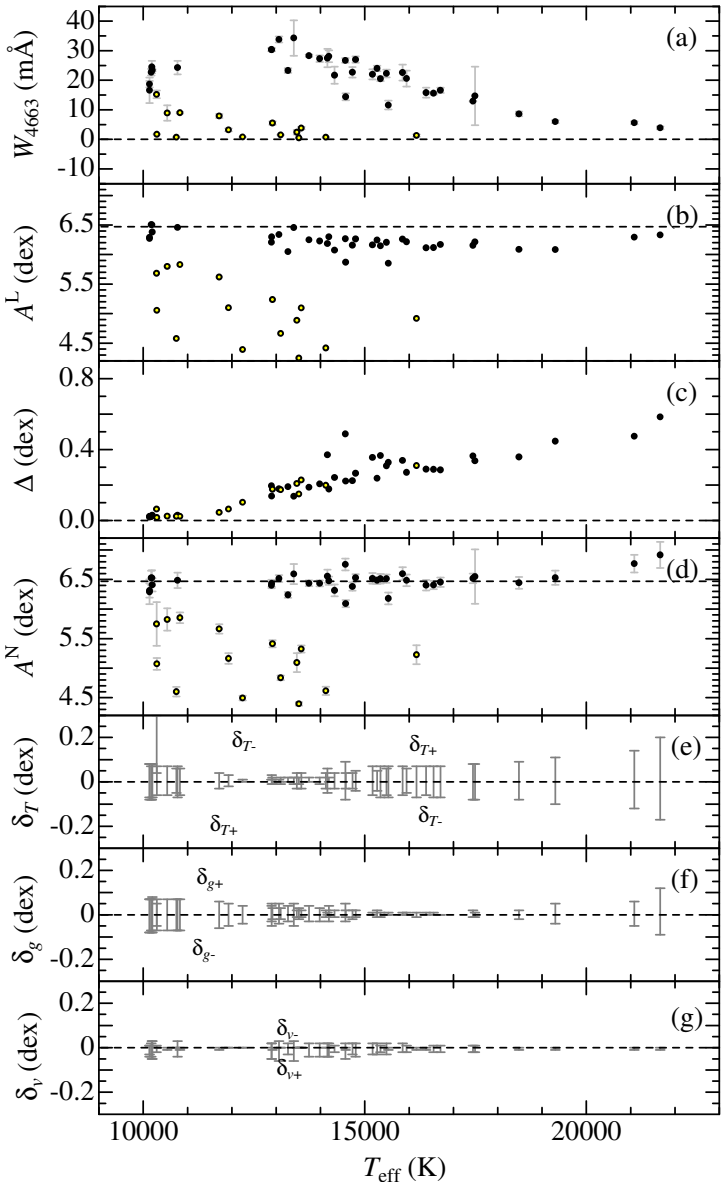

Figure 10. Abundance-related quantities for the Al II 4663 line (equivalent widths, LTE/NLTE abundances as well as NLTE corrections, and sensitivities due to perturbations of atmospheric parameters) are plotted against $T_{\rm eff}$. In panels (a)–(d), 15 chemically peculiar stars with $A^{\rm N}_{4663} < 6.0$ are distinguished by overplotting yellow small filled circles on the symbols. Otherwise, the same as in Fig. 9.

– Regarding normal B-type stars, since their Al abundances turned out almost solar as will be concluded in Sect. 5.3.1, the assumption of [Al/H] = 0 is justified.

– On the other hand, since chemically peculiar HgMn stars are considerably Al-deficient (cf. Sect. 5.3.2), applying the non-LTE departure coefficients calculated with [Al/H] = 0 is not consistent. Nevertheless, because Al abundances of such HgMn stars are not established from the problematic 6243 line (which yields only the upper limits in most cases), we have to anyhow invoke those ($A^{\rm N}_{4663}$) from the 4663 line. Then, since Δ_{4663} values are insensitive to [Al/H] (Fig. 11b), use of the [Al/H] = 0 set even in the 4663 line analysis of Al-deficient stars would not cause any serious problem.

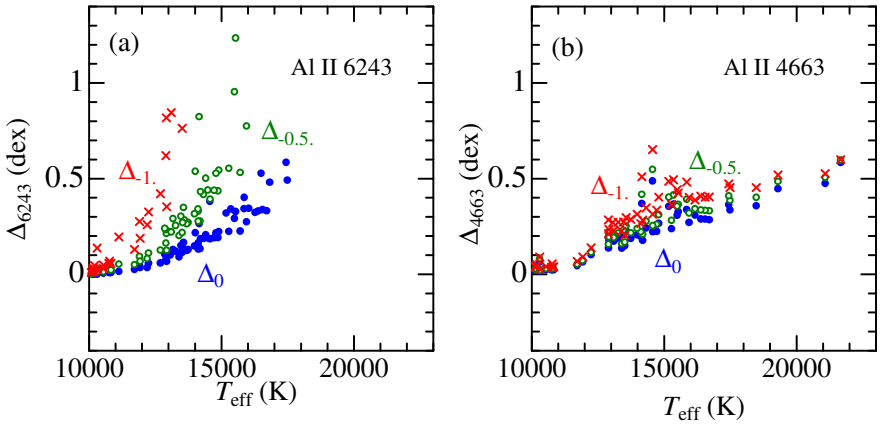

Figure 11. Test of how the non-LTE abundance correction for each star (derived from a given equivalent width) depends upon the Al abundance assumed in the statistical equilibrium calculations. Three kinds of non-LTE corrections (Δ_0, $\Delta_{-0.5}$, Δ_{-1}; depicted by filled symbols, open symbols, and crosses, respectively) are plotted against $T_{\rm eff}$, each of which correspond to different Al abundances adopted in non-LTE calculations ([Al/H] = 0, −0.5, and −1.0). Panels (a) and (b) are for Al II 6243 and Al II 4663, respectively.

5.2. Characteristics of each Al II line

Based on the results obtained in Sect. 4, we discuss the abundances derived from Al II 6243 and 4663 lines and assess their reliability and usability as abundance indicator. In addition, the problems involved with the Al II 3900 line, which was eventually abandoned to use, are also described. The discussion in this subsection is primarily confined to normal B-type stars, which may serve as a touchstone because of their prospective abundance homogeneity.

5.2.1. Al II 6243

The LTE abundances ($A^{\rm L}_{6243}$) derived from this line are considerably $T_{\rm eff}$-dependent (progressively decreasing with $T_{\rm eff}$) as shown in Fig. 9b. Although this trend is surely mitigated by applying the non-LTE corrections (Δ_{6243}; Fig. 9c), some systematic tendency remain unremoved in the non-LTE abundances ($A^{\rm N}_{6243}$; Fig. 9d), which means that they are insufficiently undercorrected. Therefore, our non-LTE calculations for this 6243 line are quantitatively still imperfect, despite that they satisfactorily predict the qualitative trend (e.g., emergence of emission feature at higher-$T_{\rm eff}$ regime; see Fig. 9a in comparison with Fig. 1a). Considering the remarkable [Al/H]-dependence of non-LTE corrections (Fig. 11). we may regard that the non-LTE results of this 6243 line are vulnerable to inadequacy in the adopted conditions (parameters) of the calculations, and thus less reliable in the quantitative sense.

5.2.2. Al II 4663

The LTE abundances ($A^{\rm L}_{4663}$) determined from the 4663 line also show some systematic tendency (decreasing with $T_{\rm eff}$; Fig. 10b). However, after the non-LTE corrections (Δ_{4663}; Fig. 10c) have been applied, this trend is almost removed in the non-LTE abundances ($A^{\rm N}_{4663}$) as can be confirmed in Fig. 10d. The exceptional outliers are two early B-type stars (HD 000886 and HD 035708) at $T_{\rm eff} \gtrsim 21000\,{\rm K}$, which might indicate that the reliability of the calculation may deteriorate at such a highest $T_{\rm eff}$ regime. The fact that the non-LTE abundances of normal B-type stars derived from this 4663 line are almost constant around $A \simeq 6.5$ over a wide temperature range ($10000\,{\rm K} \lesssim T_{\rm eff} \lesssim 20000\,{\rm K}$) suggests that this line is more reliable than the 6243 line as long as Al abundance determination is concerned. Besides, that this 4663 line is stronger (abundances are determinable even for Al-deficient stars) and does not show any apparent emission (even in early B stars) may be counted as additional evidence that this line is more advantageous than the 6243 line.

5.2.3. Al II 3900

This Al II 3900.675 line was originally selected as a potential candidate for Al abundance determination, because it was expected to have a sufficient strength (even stronger than the 6243/4663 lines) based on preparatory calculations by using the oscillator strength taken from VALD ($\log gf = -1.27$). However, observed strengths of this line in actual spectra were found to be much weaker than this expectation, suggesting the necessity of examining the reliability of $\log gf$(VALD) by checking other databases.

It was then found that, while Kurucz & Bell (1995)'s compilation presents the same value as VALD, the NIST database[8] gives a considerably lower value of $\log gf = -2.26$. Accordingly, this $\log gf$(NIST) value was eventually adopted for the Al II 3900 line in this study (cf. Table 1), which is regarded as being more reliable than $\log gf$(VALD).

Another problem involved with this Al II 3900 line is that it is severely contaminated by the neighboring Ti II line at 3900.539 Å, which is even stronger than the Al II line especially at lower $T_{\rm eff}$, though its strength drops down at higher $T_{\rm eff}$ (see Fig. 1c).

The situation mentioned above is graphically demonstrated in Fig. 12, where the observed and theoretically synthesized spectra around ∼3900 Å region are compared with each other for HD 160762 (17440 K), HD 209008 (15353 K), and HD 209459 (10204 K), which are normal stars with near-solar Al abundances of $A^{\rm N}_{4663} \sim 6.5$ (see Table 2). At any rate, this Al II 3900 line can not be used for Al abundance determinations of B-type stars because of being too weak and heavily affected by blending.

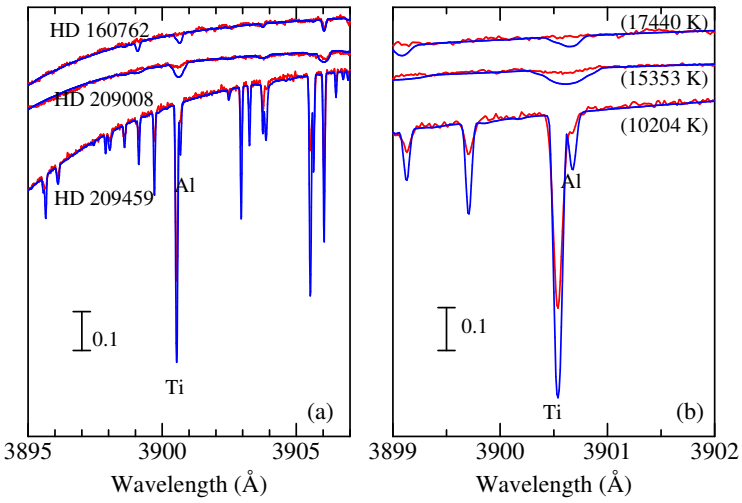

Figure 12. Observed spectra of HD 160762, HD 209008, and HD 209459 around the ∼ 3900 Å region comprising the Ti II 3900.539 and Al II 3900.675 lines (red lines) are compared with the theoretical spectra (blue lines) calculated with the solar Ti and Al abundances ($A_\odot$(Ti) = 4.99 and $A_\odot$(Al) = 6.47) under the assumption of LTE. Note that this region is on the red wing of Hζ 3889. Panels (a) and (b) are the wide view (3895–3907 Å) and the narrow view (3899–3902 Å), respectively.

[8]The Atomic Spectra Database of the National Institute of Standards and Technology. Available at https://www.nist.gov/pml/atomic-spectra-database.

5.3. Trends of Al abundances in B-type stars

In this subsection, the trends of Al abundances for normal and chemically peculiar stars are separately discussed. Here, we confine ourselves only to the non-LTE abundances derived from Al II 4663 line ($A^{\rm N}_{4663}$), which are considered to be more reliable (Sect. 5.2.2).

5.3.1. Normal B-type stars

The photospheric Al abundances of ordinary (non-CP) B-type stars should retain the composition of galactic gas from which they were formed. As mentioned in Sect. 5.2.2, the non-LTE Al abundances ($A^{\rm N}_{4663}$) turn out to be almost independent upon $T_{\rm eff}$ over a wide range of B-type stars at $10000\,{\rm K} \lesssim T_{\rm eff} \lesssim 20000\,{\rm K}$ (Fig. 10d), accomplishing a reasonable constancy. An inspection of Fig. 10d suggests that the demarcation line dividing the non-CP group (homogeneous Al abundances) and CP group (considerably Al-deficient) may be set at $A = 6.0$. Then, those 36 stars (out of 51 stars) satisfying the criterion $A^{\rm N}_{4663} > 6.0$ are regarded as normal B stars, for which the mean abundance is calculated as $\langle A^{\rm N}_{4663} \rangle = 6.47$ (standard deviation is $\sigma = 0.15$). Alternatively, if two highest-$T_{\rm eff}$ stars (HD 000886 and HD 035708) showing some deviation from the main trend (cf. Sect. 5.2.2) are excluded, $\langle A^{\rm N}_{4663} \rangle = 6.45$ with $\sigma = 0.13$.

This $\langle A^{\rm N}_{4663} \rangle$ is in remarkable agreement with the solar abundance ($A_\odot = 6.47$). That is, Al abundances of young B-type stars (representing the gas composition at the time of some $\sim 10^7$–$10^8\,{\rm yr}$ ago) are almost similar to that of the Sun (formed $\sim 4.6 \times 10^9\,{\rm yr}$ ago), which may be regarded as reasonable. Therefore, the trend of Al abundances in normal B-type stars is markedly different from the case of phosphorus (systematically subsolar by $\sim$0.2–0.3 dex in contradiction with the standard concept of galactic chemical evolution; cf. Paper II).

5.3.2. Peculiar HgMn stars

According to the demarcation in Sect. 5.3.1, those 15 stars with $A^{\rm N}_{4663} < 6.0$ are Al-deficient CP stars (yellow-dotted symbols in Fig. 10), which are mostly classified as HgMn stars (non-magnetic late B-type chemically peculiar stars). These stars are considerably underabundant in Al relative to the Sun. The extent of deficiency is diversified from star to star (by $\sim$0.5–2.0 dex; cf. Fig. 10d), though a rough tendency is observed that the anomaly tends to become more conspicuous with an increase in $T_{\rm eff}$ (from $[{\rm Al/H}] \sim -1$ around $T_{\rm eff} \sim 10000\,{\rm K}$ to $[{\rm Al/H}] \sim -2$ around $T_{\rm eff} \sim 14000\,{\rm K}$).

This is almost a reconfirmation of the trend shown in Fig. 3 of Ghazaryan & Alecian (2016), though their figure (see "Al_teff.pdf" included in their online material) indicates [Al/H] to be as low as ~ -2.5 (while the lowest [Al/H] in Fig. 10d is ~ -2), which might be due to the neglect of positive non-LTE corrections in previous determinations.

6. Summary and conclusion

Our understanding of the photospheric abundances of aluminium in B-type stars is not sufficient, despite that they may provide us with important information about the composition of galactic gas at the time of their formation. That is, previous abundance studies of this element seem to have been done more on chemically peculiar HgMn stars (late B-type), while those for relevant normal B-stars (retaining the original gas composition in their atmosphere) are comparatively scarce and do not seem to be sufficiently reliable because of the diversified results.

Motivated by this situation, a spectroscopic study was conducted to determine the aluminium abundances for 85 early-to-late B-type main-sequence stars ($10000\,\mathrm{K} \lesssim T_{\rm eff} \lesssim 22000\,\mathrm{K}$) (comprising normal stars as well as chemically peculiar HgMn stars) by using two Al II lines at 6243 and 4663 Å.

In order to take into account the non-LTE effect in the abundance analysis, non-LTE calculations were carried out on an extensive grid of models. It turned out that the non-LTE effect for these Al II 6243/4663 lines acts in the direction of line-weakening (i.e., line profile becomes shallower) caused by an overionization-induced line opacity decrease along with an enhancement of line source function, and this effect becomes more conspicuous with an increase in $T_{\rm eff}$ as well as with a decrease in $\log g$.

As for the observational data of program stars used for abundance determination, the same orange-region spectra as used in Paper II were adopted for the 6243 line, while the blue-region spectra available in the public-open database (ESO, CFHT, ELODIE) were employed for the 4663 line.

The abundance determination was carried out by the two-step process: (1) A spectrum-fitting analysis was first applied to the wavelength regions of these two lines and their equivalent widths (W_{6243} and W_{4663}) were derived from the fitting-based abundance solutions. (2) Then, non-LTE abundances/corrections as well as possible errors were evaluated from such established W values. The following conclusions are extracted from the results of Al abundances.

Regarding the non-LTE abundances of normal stars resulting from the Al II 6243 line, some $T_{\rm eff}$-dependent systematic trend remains unremoved, which means that non-LTE corrections evaluated for this line are quantitatively insufficient, despite that our non-LTE calculation reasonably reproduces the qualitative behavior of this line (e.g., appearance of emission at the higher-$T_{\rm eff}$ regime of early B-type stars).

Meanwhile, for the case of the Al II 4663 line, which is more advantageous than the 6243 line because it is stronger without showing any emission, the resulting non-LTE abundances of ordinary B stars are almost constant at the solar abundance ($A \simeq 6.5$) over the wide $T_{\rm eff}$ range ($\sim$10000–20000 K), which suggests that the abundances derived from this line are successfully non-LTE-corrected and trustable.

Therefore, according to these results derived from the Al II 4663 line, we may reasonably state that the Al abundance of the galactic gas, from which early-to-late B-type stars were born several times $\sim 10^7$–10^8 yr ago, is almost similar to the solar composition. This consequence is markedly different from the case of phosphorus (systematically subsolar by $\sim$0.2–0.3 dex; cf. Paper II).

As to the photospheric Al abundances of chemically peculiar HgMn stars (10000 K $\lesssim T_{\rm eff} \lesssim$ 15000 K), our analysis resulted that this element is conspicuously underabundant by $\sim$0.5–2 dex in comparison with the Sun (as well as normal B stars) and the extent of deficiency tends to increase towards higher $T_{\rm eff}$, which is a reconfirmation of the characteristics already reported in the past literature.

Acknowledgements. This investigation has made use of the SIMBAD database, operated by CDS, Strasbourg, France, and the VALD database operated at Uppsala University, the Institute of Astronomy RAS in Moscow, and the University of Vienna. This study is partly based on the data obtained from the ESO Science Archive Facility, ELODIE archive, and CFHT Science Archive Data (via CADC), as detailed in Table 3.

References

Allen, C. S. 1998, Abundance analysis of normal and mercury-manganase type late-B stars from optical spectra, PhD thesis, University College London, London, UK

Anders, E. & Grevesse, N. 1989, *Geochim. Cosmochim. Acta*, **53**, 197, DOI:10.1016/0016-7037(89)90286-X

Andrievsky, S. M., Spite, M., Korotin, S. A., et al. 2008, *Astronomy and Astrophysics*, **481**, 481, DOI:10.1051/0004-6361:20078837

Asplund, M., Grevesse, N., Sauval, A. J., & Scott, P. 2009, *Ann. Rev. Astron. Astrophys.*, **47**, 481, DOI:10.1146/annurev.astro.46.060407.145222

Baumüller, D. & Gehren, T. 1997, *Astronomy and Astrophysics*, **325**, 1088

Cunto, W. & Mendoza, C. 1992, *Revista Mexicana de Astronomia y Astrofisica*, **23**, 107

Fossati, L., Ryabchikova, T., Bagnulo, S., et al. 2009, *Astronomy and Astrophysics*, **503**, 945, DOI:10.1051/0004-6361/200811561

Ghazaryan, S. & Alecian, G. 2016, *Monthly Notices of the RAS*, **460**, 1912, DOI:10.1093/mnras/stw911

Golriz, S. S. & Landstreet, J. D. 2017, *Monthly Notices of the RAS*, **466**, 1597, DOI:10.1093/mnras/stw3144

Kurucz, R. L. 1993, *ATLAS9 Stellar Atmosphere Programs and 2 km/s grid, Kurucz CD-ROM, No. 13* (Cambridge, MA: Harvard-Smithsonian Center for Astrophysics)

Kurucz, R. L. & Bell, B. 1995, *Atomic Line Data, Kurucz CD-ROM, No. 23* (Cambridge, MA: Harvard-Smithsonian Center for Astrophysics)

Mihalas, D. 1978, *Stellar Atmospheres, 2nd ed.* (San Francisco: W. H. Freeman)

Monier, R. 2022, *Res. Notes AAS*, **6**, 245, DOI:10.3847/2515-5172/aca4d0

Niemczura, E., Morel, T., & Aerts, C. 2009, *Astronomy and Astrophysics*, **506**, 213, DOI:10.1051/0004-6361/200911931

Pintado, O. I. & Adelman, S. J. 1993, *Monthly Notices of the RAS*, **264**, 63, DOI:10.1093/mnras/264.1.63

Przybilla, N., Butler, K., Becker, S. R., & Kudritzki, R. P. 2006, *Astronomy and Astrophysics*, **445**, 1099, DOI:10.1051/0004-6361:20053832

Ryabchikova, T., Piskunov, N., Kurucz, R. L., et al. 2015, *Physica Scripta*, **90**, 054005, DOI:10.1088/0031-8949/90/5/054005

Takeda, Y. 1991, *Astronomy and Astrophysics*, **242**, 455

Takeda, Y. 1995, *Publications of the ASJ*, **47**, 287

Takeda, Y. 2023, *Contrib. Astron. Obs. Skalnaté Pleso*, **53**, 31 (Paper I), DOI:10.31577/caosp.2023.53.2.31

Takeda, Y. 2024, *Acta Astron.*, **74**, 43 (Paper II), DOI:10.32023/0001-5237/74.1.3

Takeda, Y. 2025, *Res. Astron. Astrophys.*, **25**, 025016, DOI:10.1088/1674-4527/adaa48